

Relationship analysis of surface roughness measurements on coatings using AFM and fractal dimension by mesoscopic model methods

A. González-Hernández, E. J. Suárez-Domínguez, Elena F. Izquierdo Kulich, A.B. Morales-Cepeda

Surface coating is a method used for protection against corrosion and environmental impact for metals. In the case of solid surfaces, coatings can be achieved by radio-frequency magnetron sputtering or other corrosion-resistant substances, which may involve the deposition of one or more layers, depending on the procedure involved, modifying the morphology of the surface and surface area. This work aims to study the relationship of two surface morphological methods through roughness and fractal dimension measurements in top-surface coatings, bilayer Ti/WTiN/WTiC (named as $n = 1$); multilayer [Ti/WTiN/WTiC] (named as $n = 40$) deposited by RF-magnetron sputtering. The measurements were obtained by profilometer and image processing pixel intensity. The topography of each coating exhibited texture with impurities as domes distributed in small cluster island types. The surface roughness were 9.42 and 18.63 nm; fractal dimension measurements were 2.55 and 2.32, respectively, with a low correlation between roughness and fractal dimension. The R-squared analysis exhibited a good relationship between the fractal dimension values, tending linear regression negative. The result of factorial design 22 confirmed the performance correlation and linear regression analyses. The fractal dimension measurements by the optical method can be great potential to evaluate surface roughness complementary in applications such as laboratories and even in scale industrial. Thus the result of statistical treatment shows high accuracy in the measurements.

Introduction

The roughness increase in the material causes the surface area to be greater than the corresponding flat surface, whose roughness value depends on the measurement technique. This difference in values is attributed to applying different physical-chemical methods based on the indirect measurement of the surface area through observing variables in direct or indirect contact whose behavior depends on the topography [1]. In coating technologies, the interface roughness represents many critical issues, and it directly controls various physical and chemical properties in deposition processes by Physical Vapor Deposition (PVD) methods [2]. The solid surface of crystalline phases presents a complex morphology, where the height changes aleatory form concerning the spatial position. These height variations are shown in the roughness of the surface and cause that surface area is more significant than the corresponding flat surface equivalent. To describe surface roughness, they use geometric information of a surface (x, y, z coordinates) using the roughness indices. Depending on how the data was explored, they always have a geometrical meaning. Some indices employ statistics to describe roughness [3]. As is well known, the analysis of the irregularities of the surface used fractal geometry [4, 5], where A_s corresponds to the surface area dimensioned from the formula described by Suarez-Dominguez *et al.* [6],

$$A_s = k(L^f) \quad (1)$$

Where k , is the parameter of the measurement precision; L , is the Euclidean length, and f , relating to the fractal dimension.

The surface fractal dimension on the mesoscopic model involves taking an image at the microscopic scale and plotting the pixel intensity profile to obtain a jagged line, which can be determined through the box-counting method the total sum of the fractal dimensions of two perpendicular lines [6]. In the present manuscript a selection of films were


grown by radio-frequency (RF) sputtering motivated for several reasons. First, the PVD significantly affects the crystal morphology that starts from a bare substrate surface nucleation, a closed, although polycrystalline film increasing roughness, which was expected to influence the fractal surface [7]. Instead, many previous works studied the influences of different sputtering conditions; e.g., Zhao *et al.* [8] reported that the surface roughness of the films was more reliable, dependent on the RF power and gas pressure. Other authors, such as Xu *et al.* [9], studied the influence of deposition parameters (argon and nitrogen gas flows) on the composition, structures, density, and topography of nitride chromium (CrN) coatings deposited by RF-magnetron sputtering. Modeling the topography evolution in terms of

A. González-Hernández 

Facultad de Ingeniería, Universidad Autónoma de Tamaulipas,
Centro Universitario Tampico-Madero zona sur
Tampico Tamaulipas, 89109, México.

E. J. Suárez-Domínguez 

Centro de Investigación, FADU. Univ. Autónoma de Tamaulipas,
Tampico, Tamaulipas, 89000, México.

Elena F. Izquierdo Kulich 

Departamento de Química-Física,
Facultad de Química, Universidad de la Habana,
La Habana, 10400, Cuba.

A.B. Morales-Cepeda 

Petrochemical Research Center, Tecnológico Nacional de
México/Instituto Tecnológico de Ciudad Madero,
Altamira, Tamaulipas, 89600, México.

Received: November 2nd, 2022

Accepted: May 15th, 2023

Published: May 22nd, 2023

© 2023 by the authors. Creative Commons Attribution

https://doi.org/10.47566/2023_syv36_1-230501

fractal parameters might shed some light on the kinetics of the growth process, including the early stage of the nucleation phenomena and subsequent diffusion of contaminants and defects along grain boundaries [10]. Literature shows enormous studies of sputter-deposited nitride titanium (TiN) coating on the substrate and surface analysis; *i.e.* information on the relationship between roughness and fractal dimension surface on a specimen of steel out coating using a system of artificial vision with two sources of light-emitting diode (LED) light illumination. This study correlated the fractal dimension with a contact profilometer's surface roughness values [11]. Nowadays, surface engineering studies focus on understanding the strong relationship between fractal analysis using the traditional method and optical-statistical processing assistance for modern science and technology [12], even the optical-statistical can propose a standardized and excellent potential methodology to evaluate surface roughness. This method can reduce costs using special equipment, essential conditions, and it time-consuming to measure [13], an alternative for researchers with limited sources, such as Latin-American countries. Our proposal study presents coatings based on carbide tungsten-titanium/nitride tungsten-titanium from ternary (Ti-W-C) to quaternary (Ti-W-C-N) compound systems deposited on the substrate according to American Iron and Steel Institute (AISI) 1060 carbon steel in the bilayer (named as $n = 1$) and forty-bilayers (named as $n = 40$) published by [14]. Depending on the characterization resource method, the increase in period deposition affects microstructure surface, promoting significative error measurements on roughness performance. Thus, this research analyzes the influence of the increased deposition time on a surface by comparing roughness and fractal dimension measurements obtained by Atomic Force Microscopy (AFM) and image processing pixels intensity (mesoscopic model). The process was developed on coatings sputtered obtained by profilometer topographical analysis, Spearman rank correlation, and linear regression statistical treatment. To evaluate the interaction of the combination between the factors and response variables of roughness average (R_a) and fractal dimension (D), at static $2k$ factorial design test was performed as a function of several layers in coatings.

Processing and analysis Details

Surface roughness measurements

The topography analyses of the coatings were carried out AFM (Nanosurf, Liestal, Switzerland), in contact mode through an Asylum Research equipment model MFP-3D (MFP-3D-Stand Alone, Asylum Research, Abingdon-on-Thames, UK) on a 2-D of $45 \mu\text{m} \times 45 \mu\text{m}$. The images were reviewed using the Gwyddion 2017 version software (Czech Metrology Institute, Brno, Czech Republic). The measurements were carried out in environmental conditions at a room temperature of 25°C . The coatings' roughness analysis was obtained with a Tesa-Rugosurf 90G Surface Profilometer (Tesa, Bugnon, Switzerland) using a diamond

cantilever radius $5 \mu\text{m}$, a contact load of 0.75 mN . The measurement was obtained on 3-D $2000 \mu\text{m} \times 1500 \mu\text{m} \times 1200 \mu\text{m}$, corresponding to one bilayer of nitride tungsten-titanium (Ti/TiWN/TiWC) named as $n = 1$, and forty bilayers (Ti/TiWN/TiWC) named as $n = 40$ deposited by RF-magnetron sputtering. The roughness profile was analyzed using lengths from 0 to $2000 \mu\text{m}$. All the measurements were repeated four times for each sample in different areas to validate the reproducibility of the data.

Fractal analysis

The surface fractal dimension is the dependent variable determined by five samples' photographs with a $1000\times$ GL digital microscope. ImageJ Software v.1.51J8 processed the final images. Each treatment process took one set of X photos; a filter was applied to decrease the characteristic roughness of the dispersion medium due to the average size of pores (in pixels) as an independent variable. The ImageJ Software determined the particle analysis function. The statistical measurements were carried to all data information by Office 365 Microsoft Excel version, using a reliability level of 95% and a significance error of 5% to all statistical treatments.

Evaluation of the fractal dimension

The authors [15], described that the model considers that due to the intrinsically random nature of the roughness, it is impossible to accurately determine the actual area of the surface, both experimentally and theoretically, where the estimated value depends on the pragmatic magnification level and the method selected for measurement. The authors define fractal geometry theory from the morphology of natural and irregular objects through fractal dimensions. The surface mesoscopic model describes the behavior of the intensity of the pixels in two directions perpendicular to each other through the image processing technique, so it is assumed that the power of the pixels is directly proportional to the height of the valleys and ridges of the surface. To determine the irregular lines in the way is used the fractal dimension (f),

$$S_F = k^{1-f_y} D_y^{f_y} k^{1-f_x} D_x^{f_x} \quad (2)$$

The fractal area of the surface (S) is estimated concerning the fractional differential calculation [15]. However, quantifying the specific fractal area (as, f) is established as a quotient between the fractal and the area equivalent to the Euclidean surface. Thus, in summary, the specific fractal (S_f) is related to the increases in surface area due to the presence of roughness for an area equivalent to a flat surface, such that the relation promotes the estimation of the fractal area [15].

Spearman Rank Correlation

The Spearman's rank coefficient (R_s) computes the responses of each of the two variables rather than their actual responses. Both nominal and ordinal data are ranked using the Spearman rank coefficient and are not restricted to either continuous/discrete variables. The ranges of the Spearman rank coefficient vary from - 1 (strong relationship negative)

to + 1 (strong relationship positive) and $R_s = 0$ (zero), representing the absence of association between variables studied. As well know, the levels corresponding when $R_s = + 1$ means a strong positive correlation; $R_s = 0.5$ indicates positive leaks; $R_s = 0$ does not exist correlation; $R_s = - 0.5$ represents a poor negative correlation; $R_s = - 1$ involves a perfect negative correlation between two dependent or independent variables [16]. The Spearman rank correlation is calculated according to [17]:

$$R_s = 1 - \frac{6 \sum_{i=1}^n D_i^2}{n(n^2 - 1)} \quad (3)$$

Where n is the number of rank pairs and D_i is the difference between a ranked pair; $D_i = R_{X_i} - R_{Y_i}$ represents the difference in ranks for each observation.

Coefficient of Determination (R^2)

R-squared (R^2) measures that part is explained in a certain variant as part of a variation, which can be predicted through the variation of the other. When the R^2 value is higher, the data describes the model better. Thus, the data consists of values $y_1, y_2, y_3, \dots, y_n$ means a response variable and a model with predictor variable is applied to the data, R^2 is determined following the eq. 4 [18].

$$R^2 = 1 - \frac{\sum_{i=1}^n (y_i - \hat{y}_i)^2}{\sum_{i=1}^n (y_i - \bar{y})^2} \quad (4)$$

Where R^2 quantifies the variable considered random through its measurement; \bar{y} determines the average in all observations, and is predicted using a fitted model. In the case of the null relationship, the predictor and response variables, y is the best “model” to explain the data. Therefore, the current conditions y_i current account for deviations in catastrophic situations: there is no existing relationship between them. The values of R^2 depend on the type selection model to fit; in standard cases like linear least-square regression model corresponding between 0 and 1. A lower value of R^2 (<0.5) indicates that the regression model is not perfect due to terms missing or the existence of substantial error variation due to a significant measurement put out [18].

Linear regression analysis

Given a data set that includes observations of the explanatory variables (x), and the response variable (y), the linear regression model calculates the relationship between the study variables considering the sample size. To fit a straight line to the scattered points on the scatterplot, simple linear regression is used, and the equation of the line is used to generate the predictions. The equation that determines the linear regression modeling is described in the following form according to [19]:

$$y_i = \beta_0 + \beta_1 x_i + e_i \quad (5)$$

Where y_i is linear equation regression; β_0 is the intercept, also called the continuous or constant; β_1 is the slope of the line; this is how much the value of x_i increases for a one-unit

increase in y_i ; e_i is the error in the model.

Factorial design 2^k

Factorial designs are essential in research, especially in the early stages of the process and/or product design development. These stages are limited when several factors are studied; otherwise, the number can extensively experiment. The study has two minimum levels to investigate the influence interactions by each factor. Consequently, various factors with two levels each will reduce the number of experiments. A factorial design with two groups is called as 2^k factorial design, which corresponds to a particular case of a multifactorial experiment. The main feature of 2^k factorial design is that it provides fewer treatment combinations in an investigation through a randomized block design. This design is used in more specific experiments considering two or more factors. When they involve a few factors, there may be no interaction between the treatment and the blocks. However, as factors increase, the possibility of the influence on the performance of the process or product is more outstanding. The 2^k factorial design encourages the experimenter to identify the significant factors that interact with each other. Subsequently, it is possible to study a complete factorial experiment with two or more levels with these important factors to determine the optimal levels for an issue, according to [20]. Since there are only two levels for each study variable, the response is assumed to be approximately linear above the element ranks. The factor levels may be quantitative or qualitative, e.g., quantitative variables are defined by two or more levels as temperature, pressure, time, etc. However, two operators define the qualitative variable: equipment from high or low factor levels.

In general terms, the following assumptions in 2^k factorial design are described as:

- The factors are invariable.
- Designs are completely randomized.
- The normality in the set data is maintained.

The two levels for each treatment or factor are usually low or high. In the two-level 2^k factorial design, the average influence of one factor is defined as the change in the response of the variable (y) produced due to a change in the level of that factor averaged over the other factor (x), (see from Eqs. 6 to 11):

Factor principal influence A:

Influence of A at the high level of factor B = $[a - (1)]/n$, the average effect of a factor in A are resumed as (eq. 6):

$$A = \frac{1}{2n} [ab + a - b - (1)] \quad (6)$$

Factor principal influence B:

Influence of B at the high level of factor A = $[b - (1)]/n$, the average influence of a factor in B are resumed in eq. 7:

$$B = \frac{1}{2n} [ab + b - a - (1)] \quad (7)$$

Factor interaction influences A and B:

The interaction influences of A and B, is (eq. 8):

$$AB = \frac{1}{2n} [ab + (1) - a - b] \tag{8}$$

Sum of squares (eqs. 9 to 11):

$$SSA = \frac{[ab + a - b - (1)]^2}{4n} \tag{9}$$

$$SSB = \frac{[ab + b - a - (1)]^2}{4n} \tag{10}$$

$$SAB = \frac{[ab + (1) - a - b]^2}{4n} \tag{11}$$

Results and discussion

Roughness analysis

Figure 1(a-f) shows the roughness and topography of n=1 and n=40 in coatings obtained by RF-magnetron sputtering. Figure 1a shows the roughness profile of n=1, measuring a coating thickness of $2.06 \pm 0.06 \mu\text{m}$. Figure 1c shows the topography in the 3-D coating and observes parallel lines reaching an altitude up to $1.2 \mu\text{m}$, probably attributed to substrate preparation in previous rough paper sand. Figure 1e observes the presence of crest (or domes) distributed as a small cluster, as like-wise, it observes some imperfections due to the contribution of carbon steel substrate roughness. The topography observed natural texture, exhibiting certain homogeneity of grains with equal dimensions. The R_a measurements by AFM analysis expressed in the mean nanometer of coating roughness is $18.63 \pm 0.01 \text{ nm}$.

Conversely, Figure 1b shows the roughness profile of n=40, measuring a coating thickness of $3.29 \pm 0.12 \mu\text{m}$. Figure 1d shows the topography is notable the uniform smooth texture with null ridges or large grains, presenting a decrease in the roughness of $9.42 \pm 2.89 \text{ nm}$ in the n=40 system, similar to [21]. Figure 1f observes the presence of crest (or domes) distributed as a small cluster, as like-wise, it observes some imperfections due to the contribution of rough substrate (carbon steel); this characteristic is also shown in Figure 1e. The roughness reduction is due to the grain refinement of the multilayer coating, attributed to the low deposition periods [22]. Authors [23], mention that the grains refinement is due to the ion bombardment that stimulates the bilayers, many nucleation sites during growth are formed, promoting the reduction in the individual thickness of each layer and the number of bilayers increases, implying a decrease in surface roughness. The orange skin texture surface is probably due to the formation of dense coatings without pores and morphological cauliflower-like inclusions, typical in sputtering processes and randomly distributed [24].

The particles dispersed on surface coating are due to a high rate plasma sputtering process producing particles disclosed. The process causes at least a part of the sputtered target atoms' ionization. It is performed at such a parameter that the pick-up probability of ionized sputtering target atoms on the surface of grains is high [25]. The size grain decreases when the number of layers increases, and the texture is softer and smoother [26].

Fractal dimension analysis

Images with from 50x to 1000x magnification of the solid surfaces were treated using two different coatings growths obtained using a rf magnetron sputtering technician. Figure 2a shows the substrate without treatment, presenting surface

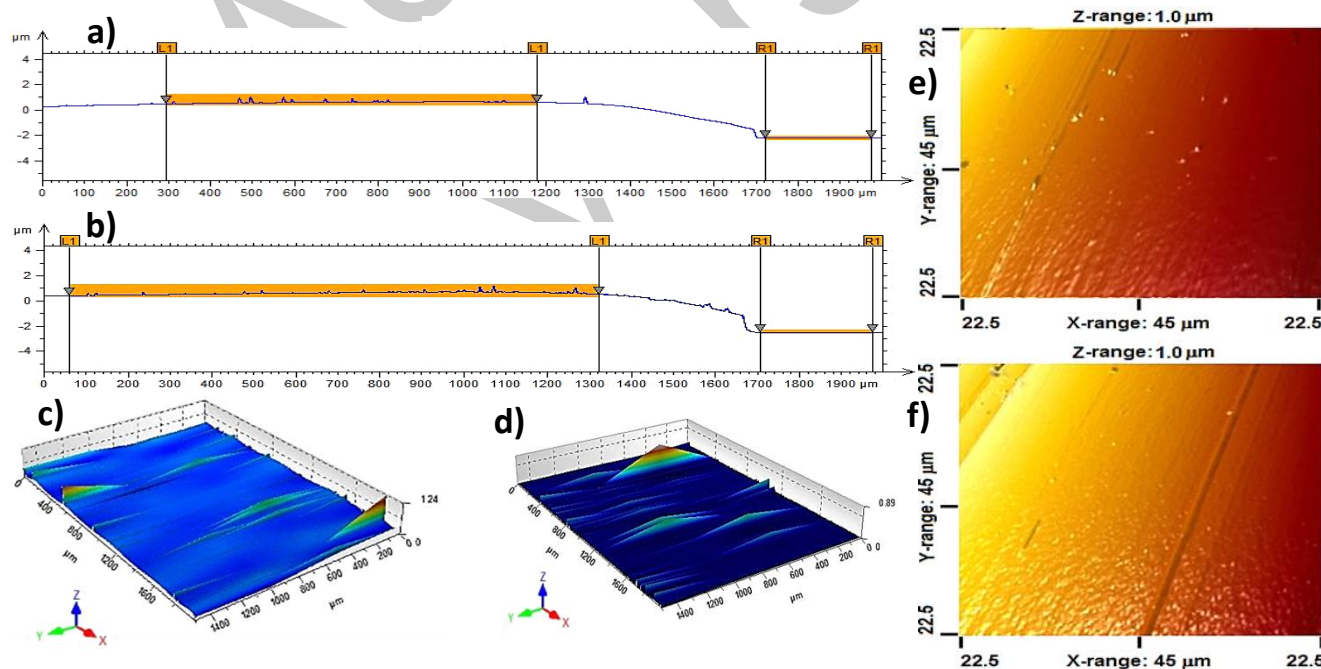


Figure 1. Images of topography and roughness in n=1 and n=40 coatings deposited by RF-magnetron sputtering; (a,b) Roughness profile by profilometer; (c,d) Plotting in 3-D images obtained by profilometer; (e,f) Plotting in 2-D images obtained by AFM

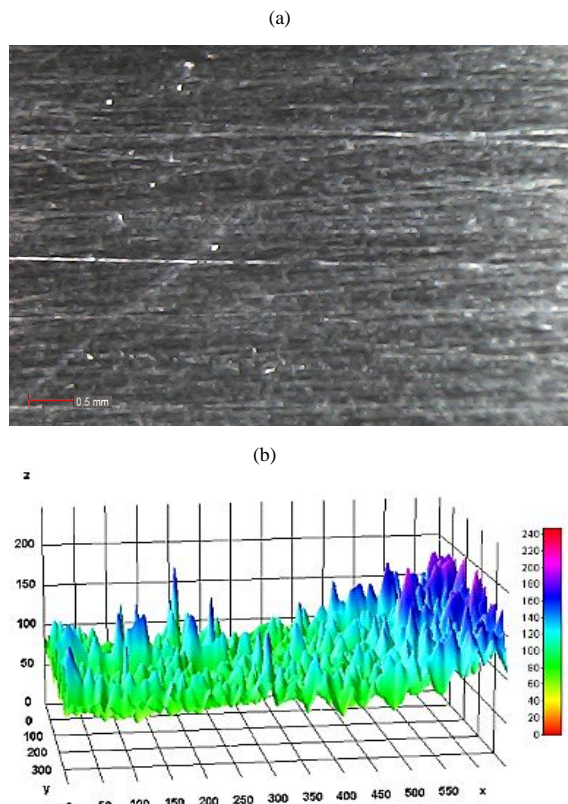


Figure 2. Images of the process of fractal dimension in a substrate or without treatment; (a) Image of the substrate without treatment captured in GL digital microscope at 1000x (58.9x magnification); (b) 2D plotting through image processed using ImageJ Software for surface reconstruction.

lines due to the preparation of the substrate without the polishing process. Figure 2b shows the image reconstruction to obtain a fractal dimension by profile analysis, calculating (D) 2.42.

Figure 3 shows the fractal value's dimension on an n=1 coating. In Figure 3a, the bilayer has a rough surface texture. This structure is the one that allows us to recognize the formal surface differences that are related to the fractal dimension values, also presented in Figure 3b. The image reconstruction is shown to obtain a fractal value $D = 2.55 \pm 0.128$. This structure is the one that allows us to recognize the formal surface differences that are related to the fractal dimension values, also presented in Figure 3b. The image reconstruction is shown to obtain a fractal value $D = 2.55 \pm 0.128$.

Figure 4 shows the surface and roughness profile in 2-D and 3-D for the n=40 coating. Figure 4a observes the reduction of surface imperfections, smooth texture, and some parallel lines attributed to the preparation of the substrate, as shown in the AFM image. In Figure 4b, the 2-D image indicates the sections with imperfections by cut analysis. From the picture, the reconstruction obtains a fractal value $D = 2.32 \pm 0.116$.

Correlation coefficient of Spearman Rank

The state of the null hypotheses to evaluate if exists a difference between means dimension fractal and profilometry in n = 1 and n = 40 coatings deposited by RF-

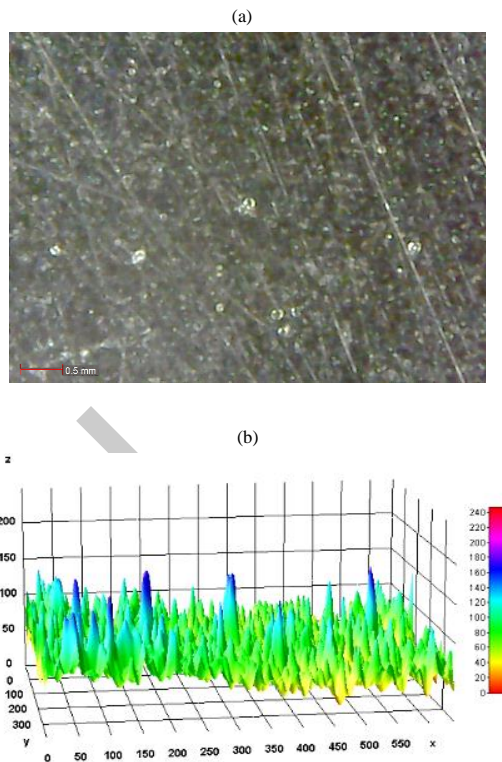


Figure 3. Images of the fractal dimension process in the substrate or with TiWN / TiWC bilayer coating; a) Image captured to GL 1000x digital microscope (59.8x magnification) ; b) Plotting in 2D obtained using ImageJ Software.

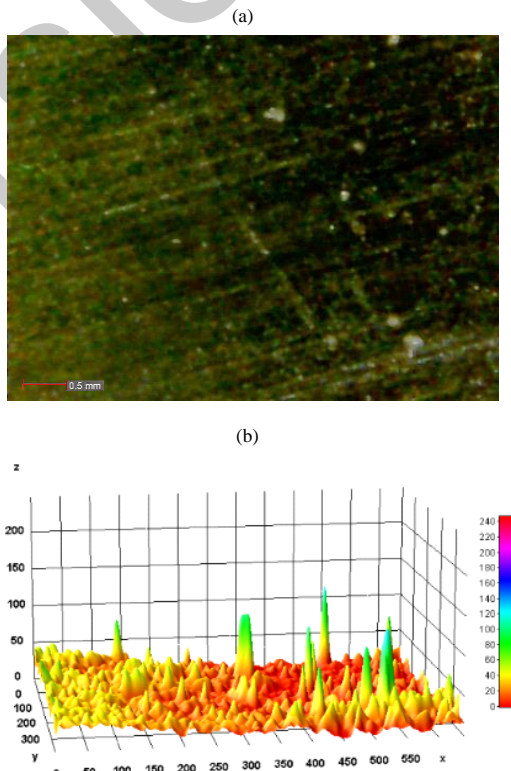


Figure 4. Images of the fractal dimension process in the substrate or with forty-bilayers coating; a) Image captured to GL 1000x digital microscope (59.8x magnification); b) Plotting in 2-D and (c) 3-D obtained using ImageJ Software.

Table 1. Shows the estimated fractal dimension (D) and surface roughness in n=1 and n=40 coatings, measurements four replicates each by type material.

Type material	Roughness, Ra (nm)							Fractal dimensión, D						
	Sample (n)				Statistical estimation			Sample (n)				Statistical estimation		
	1	2	3	4	Mean	Standard Deviation	Standard Error	1	2	3	4	Mean	Standard Deviation	Standard Error
n=1	24	10.4	13.6	26.5	18.63	6.78	3.39	2.59	2.54	2.56	2.52	2.55	0.03	0.01
n=40	6.76	12.3	7.1	11.5	9.42	2.50	1.25	2.32	2.31	2.33	2.32	2.32	0.01	0.00

magnetron sputtering. Thus, the states nulls hypotheses are:

- H0: The means of surface measurements obtained by profilometry and fractal dimension by the mesoscopic model are equal ($\rho_1 = \rho_2$).
- H1: The means of surface measurements obtained by profilometry and fractal dimension by the mesoscopic model are different ($\rho_1 \neq \rho_2$).

Table 1 shows the roughness and fractal dimension values in n=1 and n=40 coatings, statistical estimation such as mean, standard deviation, and standard error. For the case of roughness measurements, it observes significant variance between the values. The roughness values of coatings are substantial according to the microscope used, especially in the high-magnification scale [27]. However, the fractal dimension values present less standard deviation than the measurement precision for a parmagnification image [28]. The statistical estimation of standard deviation and error in fractal dimension shows a minimum difference from 0.00 to 0.03, indicating high accuracy in the development method.

The ranking is assigned from 1 to 8, to Roughness and Fractal dimension values, ordering from the smallest to the largest in n=1 and n=40 coatings; e.g. the roughness value of 24.00 nm has the rank 7, while the Fractal dimension for the same measurement (2.59) has a rank of 8, and their difference (d) is -1 (see Table 2). Table 2 shows rankings forit calculates the differences (d) between the ranges found from roughness and fractal dimension. The difference is elevated to squared (d)², and the differences are added (Σ). Finally, the correlation coefficient of Spearman ranges (R_s) is determined while the value is 0.4643, indicating positive leak dependence; the magnitudes of the ranks of one variable are independent of the magnitudes of the ranks of the second variable y [29].

From the eq. 8, the correlation coefficient of Spearman ranks (R_s) was calculated using an extension number of replicates total, n = 8.

Linear regression and determination coefficient

Figure 5 shows the R-squared (R²) measure of the proportion of the variance for a dependent variable explained by two independent variables corresponding to fractal dimension values and surface roughness in coatings n=1 and n=40 obtained by RF-magnetron sputtering. It observes a high R-squared for fractal dimension (R² = 0.8116,

corresponding to 81.16%), indicating that the stock performance moves relatively in line with the index with $y = -0.0463x + 2.6446$ linear regression. However, the roughness presented a low R-squared (R² = 0.2562, corresponding to 25.62%), indicating the security does not generally follow the index's movements with $y = -1.5195x + 20.858$ linear regression [30]. The linear regression indicates the moderate independence of variables; however, their tendency can generate interaction in the future [31]. AFM methods, indicated by R²-square can be great potential in combination with statistical and other measurements in industry and production laboratories. Structured surface, complex time series, and difficulty describing dividing lines are much more common than can be expected [32].

Table 2. Assignment of ranges to original values.

Type material	Roughness, Ra (nm)	Rank	Fractal dimension (D)	Rank	Difference (d)	(d) ²
n=1	24.00	7	2.59	8	-1	1
	10.40	3	2.54	6	-3	9
	13.60	6	2.56	7	-1	1
	26.50	8	2.52	5	3	9
n=40	6.76	1	2.32	2	-1	1
	12.30	5	2.31	1	4	16
	7.10	2	2.33	4	-2	4
	11.50	4	2.32	2	2	4

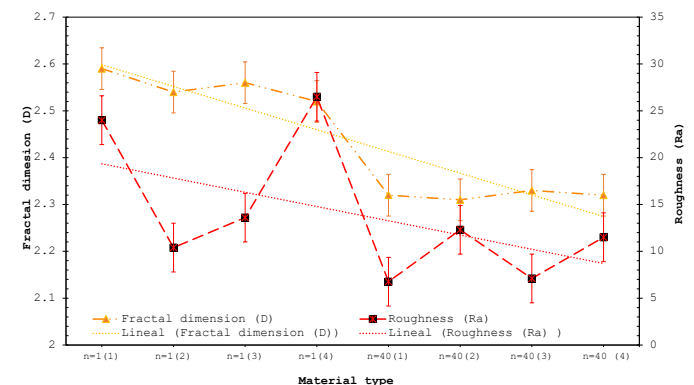


Figure 5. Plotting of behavior the linear fixed regression on n = 1 and n = 40 coatings.



Table 3. From data of Table 2 is organized the treatment combination (roughness and fractal dimension values)

Treatment combination			Replicate			
A	B	Treatment	1	2	3	4
-	-	(1)	24.00	10.40	13.60	26.50
+	-	A	6.76	12.30	7.10	11.50
-	+	B	2.59	2.54	2.56	2.52
+	+	AB	2.32	2.31	2.33	2.32

2² Factorial design Treatment statistical

Its called 2² because the factorial design is two factors (A and B). Statements of hypothesis for process statistical considered such variables factor A (two types of material) and factor B (two types of method). Thus, the states nulls hypotheses are:

Factor A

- H0: Exist is a factor principal influence of A on the dependent variable
- H1: Exist is no factor principal influence of A on the dependent variable

Factor B

- H0: Exist is a factor principal influence of B on the dependent variable
- H1: Exist is no factor principal influence of B on the dependent variable

Interactions

- H0: Exist a interaction significantly between factors
- H1: No exist interaction significantly between factors

Considering the previous investigation into the influence of performance roughness and the dimension of the fractal measurement on coating [11]. The performance roughness is factor A, and the two interest levels are n=1 and multilayer. The fractal dimension is factor B, with the high level denoting n = 1 and the low level meaning multilayer coating. The experiment is replicated four times, so there are 16 runs.

From Table 2, the order in which the runs are made is random, so this is a completely randomized experiment (Table 5).

Table 4. Data for problem from Table 2

Treatment	Factor influences value	Sum of squares
A	- 4.72	89.16
B	- 11.58	536.73
AB	4.49	80.60

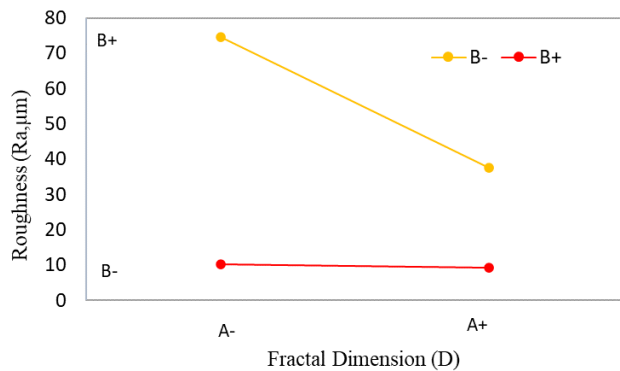


Figure 6. Plot of interaction influence on roughness and fractal dimension measurements.

Table 5. Two-way ANOVA analysis.

Source of variation (Type of material)	Sum of squares	Degrees of freedom	Mean square	F ₀	F _{α,(a-1),(ab)(n-1)}
n=1 (A)	89.16	1	89.16	5.12	4.75
n=40 (B)	536.73	1	536.73	30.83	4.75
Interaction AB	80.60	1	80.60	4.63	4.75
Error	208.89	12	17.41	-	-
Total	915.38	15	-	-	-

α=0.05, R.L.=95%

Determining the factor and computation of sum squares

The expression from Eqs. 10 to 16 determines the relation and interaction of variables. Table 6 shows the values of the influence of A and B corresponding to negative relation; however, the interaction between the response variables is good relation of 4.49. The sum of squares exhibits a good relation between variables. Figure 6 illustrates the typical plot of influence. The graph demonstrates that process parameter surface morphology and the interaction between “roughness and fractal dimension” are statistically significant at a 5% significance level [33]. In other words, the tendency of lines to predict a possible interaction (AB) is similar to the one obtained through linear regression analysis, indicating a negative interaction.

Hypothesis test by D. Fischer

It calculates the F-Fischer statistics (F₀) using the analysis of variance (ANOVA) statistically by the sum of least squares. Table 7 is summarized below.

To carry the contrast process is considering the decision rule to determine the outcome for each of the three alternative hypotheses, were mentioned:

If $F_0 < F_{α,(k-1),(k-1)(b-1)}$, then, the null hypothesis is accepted; otherwise, the alternative is accepted.

Table 5 shows the F_α (treatment of n = 1 and n = 40) in this case. The independent influences are significant differences in yield the surface methods, is say, does not exist strong relation significative between type material. However, the interaction of responses variables has interaction since the null hypothesis is accepted considering a reliability level (R.L.) of 95% and significance error (α) of 5%, evidenced a leak interaction between study factors. This characteristic means that the influence does not differ between the factor levels. In this case, the two simple influences of a given factor are equivalent and thus can be more simply described by collapsing then into a single main influence [34].

Conclusions

With the analysis of composition and number of layers of the metallic surface, we carried out an experimental study analyzing coating presence affectation to the morphology on the microscopic and mesoscopic scales, estimating the surface area from the box-counting fractal dimension determined from images taken on the mesoscopic scale. To the carrier study were used two coating types: Ti/WTiN/WTiC (named as n = 1); multilayer [Ti/WTiN/WTiC] (named as n = 40). The result showed that the topography exhibited few domes distributed as small



clusters, each surface coating. The roughness (R_a) and fractal dimension (D) measurements ranged from 9.42 to 18.63 and 2.55 to 2.32, respectively. The relationship between the roughness and fractal dimension is shown 0.4643 by Spearman ranks (rs). The $R^2 = 81.16\%$ coefficient indicated that the stock performance moves relatively in line with the index, which was considered acceptable for the model limitations, the experimental errors, and the assumption that the fractal dimension itself can be considered a stochastic variable value on its spatial position. The linear regression indicated moderate variables independence; however, the negative tendency will predict possible interaction. This behavior is according to the found in factorial design 2k analysis, assuming does not exist strong relation significative between type material. However, the interaction of responses variables has interaction since the null hypothesis is accepted considering a reliability level of 95% and significance error of 5%. The fractal dimension measurements by the optical method can be a great potential to evaluate surface roughness complementary in applications such as laboratories even, in scale industrial, thus that result of statistical treatment shown high accuracy in the measurements.

Acknowledgements

A. González-Hernández acknowledges Consejo Nacional de Ciencia y Tecnología (CONACYT-México, 2017) for a “Beca Mixta, Movilidad al Extranjero” scholarship (No. 291212). They also appreciate the facilities provided by the laboratory to obtain the hard coatings and AFM facilities of the University of Valle, Cali Colombia, and GIDEMP group of SENA-ASTIN.

References

- [1]. D. Farin, D.J. Avnir, *Phys. Chem.*, **91**(1987) p.5517–5521
- [2]. Z. Yiping, W. Gwo-Ching, L. Toh-Ming, Yiping Zhao, Gwo-Ching Wang, Toh-Ming Lu, in *Experimental Methods in the Physical Sciences*, Academic Press, **37**, (2001) p.309-351.
- [3]. M. Hollaus, *A review of surface roughness concepts, indices, and applications*, (2014).
https://www.newfor.net/wp-content/uploads/2015/02/DL15_NEWFOR_Roughness_state_of_the_art.pdf (accessed on 24 April 2021)
- [4]. S. Kulesza, M. Bramowicz, *Appl. Surf. Sci.*, **293** (2014), p. 196–201.
- [5]. M. Babič, M. Cali, I. Nazarenko, C. Fragassa, S. Erinovic, M. Mihaliková, M. Janić, I. Belič, *Int. J. Interact.*, **13** (2019) p. 211–219.
- [6]. E.J. Suárez-Domínguez, A. Perez-Rivao, M.T. Sanchez-Medrano, J.F. Perez-Sanchez, E. Izquierdo-Kulich, *Surf. Interfaces* **18** (2020) p. 100407
- [7]. P. Triloki, D. Sinhg, T. Srivastava, *Geomatics Nat. Hazards Risk* **1**, (2010) p. 243–257.
- [8]. Y. Zhao, Y. Qian, Z. Yu, W. Chen, *Thin solid films* **286**, (1996) p. 45–48.

- [9]. J. Xu H. Umehara, I. Kojima, *Appl. Surf. Sci.*, **201** (2002) p. 208–218.
- [10]. M.A. Tsysar', *J. Superhard Mater.*, **34** (2012) p. 256–263.
- [11]. J.G. Ayala-Landeros, V.M. Castaño-Meneses M.B. Becerra-Rodriguez, S. Servín-Guzman, S.E. Román-Flores, J.M. Olivares-Ramírez, *Comp. y Sist.*, **22**, (2018) p. 1473–1485.
- [12]. W. Zhou, Y. Cao, H. Zhao, Z. Li, P. Feng, F. Feng, *Fractal Fract.* **6**, 3 (2022) pp. 135.
- [13]. D. Xu, Q. Yang, F. Dong, S. Krishnaswamy, *J. Eng.*, **9** (2018) p. 773–778.
- [14]. A. González-Hernández, A.B. Morales-Cepeda, M. Flores, J.C. Caicedo, *Coatings* **11**(7), (2021) p. 797.
- [15]. A. González-Hernández, E.J. Suárez-Domínguez, W. Aperador, A.B. Morales-Cepeda, E.F. Izquierdo-Kulich, J.C. Caicedo, *Surface Review and Letter*, **6** (2022) p. 1–15.
- [16]. P. Schober, Ch. Boer, L.A. Schwarte, *Anesth. Analg.*, **126**,5 (2018) p.1763–1768.
- [17]. J.P. Verma, G. Abdel-Salam, In: *Nonparametric Correlations (Hoboken USA: John Wiley & Sons, 2019) p. 175–191.*
- [18]. H. Pham, *Mathematics* **7**,12 (2019) p. 1215.
- [19]. M. Tranmer, M. Elliot, Multiple Linear Regression, (2020), Available: *Multiple regression Tuesday 20th Jan 2004* (accessed on 28 May 2021)
- [20]. K. Krishnaiah, P. Shahadudeen, In: *The 2k Factorial Experiments* (New Delhi: PHI Learning Private Limited, 2012) p. 110–139. ISBN 978-81-203-4527-0
- [21]. M.I. Yousaf, V.O. Pelenovich, B. Yang, C.S. Liu, D.J. Fu, *Surf. Coat.* **282** (2015) p. 94–102
- [22]. B. He, L. Zhang, X. Yun, J. Wang, G. Zhou, Z. Chen, X. Yuan, *Coatings* **12**, 3 (2022) p. 307.
- [23]. J.C. Caicedo, C. Amaya, L. Yate, L.M.E. Gómez, G. Zambrano, J. Alvarado-River, J. Muñoz-Saldaña, P. Prieto, *Appl. Surf. Sci.*, **256**, 20 (2010) p. 5898–5904.
- [24]. P.R.T. Avila, E.P. da Silva, A.M. Rodrigues, K. Aristizabal, F. Pineda, R.S. Coelho, J.L. Garcia, F. Soldera, M. Walczak, H.C. Pinto, *Sci. Rep.* **9**, 15898 (2019).
- [25]. J.T. Gudmundsson, *Plasma Sources Sci. Technol.*, **29** (2020) p.113001.
- [26]. M.A. Gómez, G. Bejarano, D. Cano, J.A. Osorio, F.J. Bolivar, *Rev.EIA.Esc.Ing.Antioq.* **16**, (2011) p. 93–102
- [27]. A. Gujrati, R.K. Subarna, P. Lars, D.B.Tevis Jacobs, *ACS Appl. Mater. Interfaces* **10**,34 (2018) p. 29169–29178.
- [28]. X. Zuo, X. Tang, Y. Zhou, Chaos, *Solitons & Fractals*, **135** (2020) p.109755.
- [29]. J.H Zar, Spearman Rank Correlation, *Encyclopedia of Biostatistics*, (eds P. Armitage and T. Colton).
- [30]. J.S. Cramer, *J. Econom.*, **35** 2-3 (1987) p. 253–266.
- [31]. M.R. Mahmoudi, M. Mahmoudi, E. Nahavandi, *Communications in Statistics-Theory and Methods*, **45**(21), pp.6284-6289.
- [32]. V. Hotar, P. Salac, *Sci. World J.*, **2014** (2014) p. 1-10.
- [33]. J. Antony, In: *Full factorial designs (Edinburgh Scotland UK: Elsevier, 2014) p. 63–85*
- [34]. A.V. Frane, *Adv. Meth. Pract. Psychol. Sci.* **41**, (2021) p. 1–20